Milestone Report #1: MSR (Manifold Switching Reactor) Studies

Project Name: ***3-1110-0089***
Project Name: ***Chemical Looping Oxygen Generation for Oxy-Fuel Combustion and Gasification***

AUTHORS:
Prof. Behdad Moghtaderi
Prof Terry Wall
Dr Elham Doroodchi
Dr Kalpit Shah
Dr Jafar Zanganeh
Mr Hui Song

Priority Research Centre for Energy
Faculty of Engineering & Built Environment
The University of Newcastle

University of Newcastle
6/13/2012

Acknowledgements: *The authors wish to acknowledge financial assistance provided through Australian National Low Emissions Coal Research and Development (ANLEC R&D), NSW Coal Innovation, and Xstrata Coal Research Limited. ANLEC R&D is supported by Australian Coal Association Low Emissions Technology Limited and the Australian Government through the Clean Energy Initiative.*

I, the undersigned, being a person duly authorised by the Grantee, certify that:

(a) the above information is true and complete;

(b) the expenditure of the Funding received to date has been solely on the Project;

(c) there is no matter or circumstances of which I am aware, that would constitute a breach by ANLEC R&D or, if applicable the End Recipient, of any term of the Funding Agreement between ANLEC R&D and the Grantee dated [insert date] that has not been notified by the Grantee.

Signature: B Moghtaderi

Position: Project Leader (Head, Chemical Eng, The University of Newcastle)

Name: Professor Behdad Moghtaderi

Date: Draft version for review 12 June, 2012
Final version after revisions 25 Nov 2012

Table of Contents

List of Figures

List of Tables

EXECUTIVE SUMMARY

This report details the technical progress made in the project "*Chemical Looping Oxygen Generation for Oxy-Fuel Combustion and Gasification*" under the milestone task "manifold Switching Reactor (MSR)" studies. The report covers the technical achievements in a number of areas including:

- Development of experimental setups (both bench- and pilot-scales)
- The impact of MSRs on metal oxides redox reactions

Overall, the progress made thus far in the above areas is on time and budget and in some cases well ahead of the agreed schedule.

1. TECHNICAL BACKGROUND

Oxygen is the second largest-volume chemical produced in the world with a 30% share of the global industrial gas market. The global demand for oxygen in 2011 is forecast to be 950 billion cubic meters with an annual growth rate of about 6%. It has major commercial applications in metallurgical industry, chemical synthesis, glass manufacturing, pulp and paper industry, petroleum recovery / refining, and health services. Emerging markets for oxygen include advanced power generation systems, such as integrated gasification combined cycle (IGCC), oxy-fuel combustion and solid oxide fuel cells, SOFC. Among these, oxy-fuel combustion is particularly an attractive low emission technology because of its inherent ability for in-situ separation of CO_2. However, oxy-fuel combustion requires oxygen and, thereby, an air separation unit (ASU) to function effectively. Conventional ASU units (e.g. cryogenic systems) may consume between 10% and 40% of the gross power output of a typical oxy-fuel plant and constitute 40% of the total equipment cost (about 14% of the total plant cost).

Oxygen is commonly produced at industrial scales by air separation using cryogenic distillation and adsorption based technologies (pressure swing adsorption, PSA, and vacuum-PSA or VPSA). Advanced technologies such as membrane separation (e.g. ion-transport membrane, ITM) and in-situ air separation are also being developed for small-volume point-of-use oxygen generation. Cryogenic processes are generally expensive owing to the energy intensity of their air compression sub-process. Similar to the cryogenic methods, air compression is a key step in the adsorption based air separation methods and as such the specific power consumptions of PSA and VPSA plants are not much lower than their cryogenic counterparts. Membranes have been in commercial use for several decades but much of their past applications have been in liquid-liquid and liquid-solid separation. The use of membranes for large volumetric gas flow rates, such as those in air separation, has not been demonstrated yet. Membrane systems also suffer from high cost of manufacture. There is a need for a more simple and cost effective air separation technology with much smaller energy footprint and lower capital cost than conventional and emerging air separation methods.

In recognition of this need our group has been developing two chemical looping based methods for air separation. The first method known as chemical looping air separation (CLAS) is a general technique for tonnage production of high purity oxygen while the second method (integrated chemical looping air separation, ICLAS) is a modified version of the CLAS process specifically tailored for oxy-fuel applications. The integrated chemical looping air separation (ICLAS) process is a step-change improvement over the CLAS process and has been specifically tailored for ease of integration with oxy-fuel type power plants running on organic (e.g. biomass) or fossil-based (e.g. coal, gas, oil, etc) fuels. For example consider an oxy-fuel coal-fired power plant where coal, oxygen (from the ASU) and recycled flue gas are co-fed into the boiler and the mixture is combusted at high temperatures. The heat generated from the combustion process runs a steam cycle which in turn converts the thermal energy into electricity. The use of recycled flue gas here is an important and integral part of the oxy-fuel combustion process because firing pure oxygen in a boiler would result in excessively high flame temperatures which may damage the boiler. Therefore, the mixture must be diluted by mixing with recycled flue gas before it can be fed into the boiler. Given the need for recycled flue gas in oxy-fuel combustion and considering the high energy demand for steam generation in a CLAS type process, recycled flue gas rather than steam is employed in the ICLAS process during the reduction phase

(Figures 1 and 2). This innovative use of the recycled flue gas in the ICLAS process: (i) lowers the overall energy footprint of the air separation process and hence operational costs to levels well below those of the CLAS process, (ii) simplifies the hardware required for chemical looping air and thereby reduces the capital cost for the air separation unit in an oxy-fuel power plant, and (iii) leads to a more effective integration of the ASU with the oxy-fuel plant due to better use of material and energy streams (see Figure 2).

The working principle of the ICLAS process is similar to that of the CLAS process but the ICLAS process is executed is a distinctly different way. Both CLAS and ICLAS processes works in a cyclic fashion by continuous recirculation of metal oxide particles between a set of two interconnected rectors, where oxidation (R1, O_2 coupling) and reduction (R2, O_2 decoupling) of carrier particles take place, respectively. In both processes air is first fed into the oxidation reactor for separation of oxygen from air through the oxygen coupling process (i.e. regeneration of reduced carrier particles) and then the oxidised (i.e. regenerated) particles are reduced in a reduction reactor to release oxygen via the oxygen decoupling reaction. However, in the ICLAS process the reduction and hence oxygen decoupling process takes place in the presence of recycled flue gas not steam. The mixture of oxygen and recycled flue gas exiting the reduction reactor is then directly fed into the boiler of the oxy-fuel plant (Figure 3). The use of flue gas rather than steam not only eliminates the need for steam generation but also implies that condenser units for separation of O_2 from steam are no longer required. This reduces the number of unit operations and thereby capital cost as well as operational and running costs.

From the energy efficiency point of view the heat transported by the incoming carrier particles into the reduction reactor is sufficient to support the endothermic oxygen decoupling process. In practice, though, some heat must be supplied to the reduction reactor to compensate for heat losses to the surrounding. However, unlike the CLAS process no additional heat is also required for generation of superheated steam in the ICLAS process. Moreover, much of the required heat duty is offset by utilising the flue gas stream which is already hot. Our preliminary calculations suggest that the heat demand for the ICLAS process is ≈0.03 kWh per cubic meters of oxygen produced (i.e. 0.03 kWh/m^3_n) which is about 30% and 90% less than those of the equivalent CLAS and cryogenic type process, respectively.

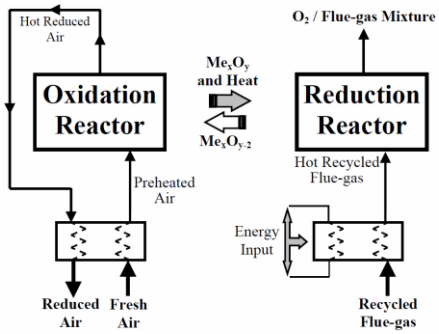

Figure 1: Schematic of the ICLAS process.

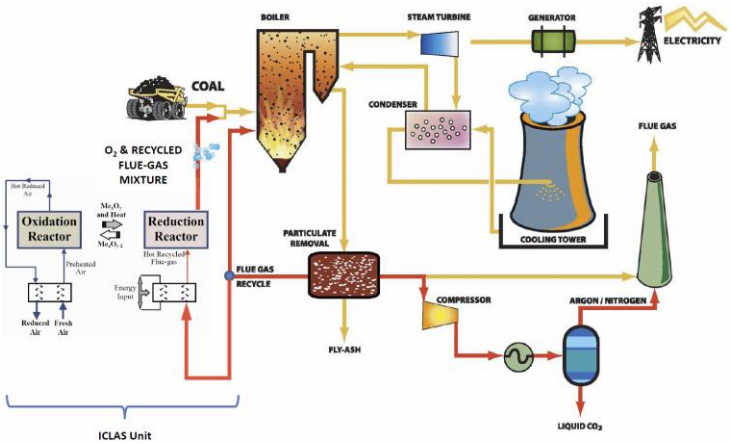

Figure 2: Schematic of an oxy-fuel coal-fired power plant retrofitted with an ICLAS unit.

2. BRIEF PROJECT & MILESTONE DESCRIPTIONS

This project is part of a larger program of study underway at the University of Newcastle on alternative air separation technologies and specifically complements two other relevant projects funded by the NSW Coal Innovation and Xstrata Coal Research Ltd, respectively. As Figure 3 shows, the major research elements of this program are: (i) fundamental studies, (ii) integration & adaptation studies, and (iii) demonstration. The emphasis of the NSW Coal Innovation is mainly on fundamental studies at bench- and pilot-scales under controlled laboratory settings whereas the ANLEC-R&D project (this project) exclusively focuses on practical issues related to integration and adaptation of CLAS type air separation units into conventional combustion and gasification plants. The Xstrata project complements both NSW and ANLEC projects. Demonstration element will be a future project to be formulated after completion of current projects and in conjunction with a LETC demo (e.g. Callide project).

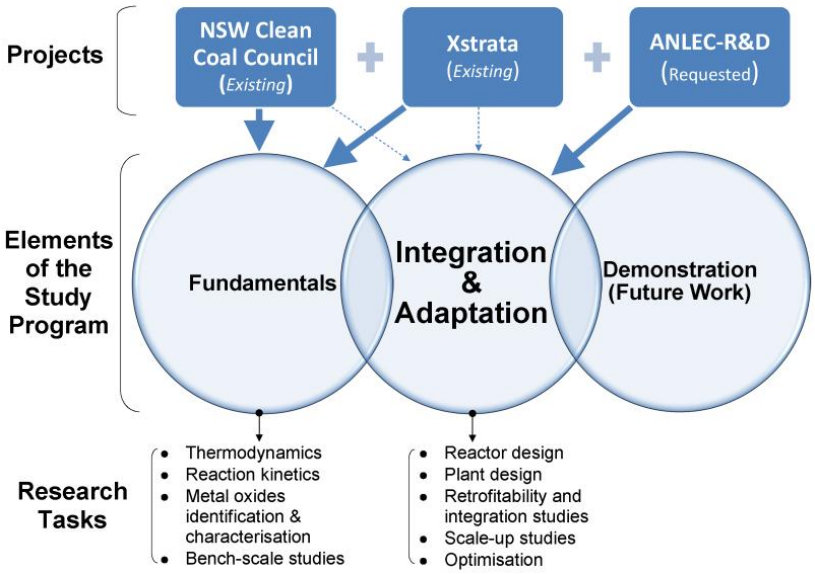

Figure 3: Relationship between the existing ANLEC, NSW and Xstrata chemical looping projects.

The material provided in the present report briefly summarises the technical progress made on MSRs and their impact on redox reactions of metal oxides. The rationale behind MSR studies is to resolve the issues associated with solid transport with an emphasis on developing novel reactors. Note that chemical looping systems commonly consist of two interconnected fluidised bed reactors through which metal oxide particles are circulated. Adoption of this configuration for large-scale operations may lead to a series of challenges such as: (i) blockage of connecting pipes, (ii) undesirable fluctuations in particle inventory within each reactor, (iii) particle loss, segregation and fragmentation, (iv) degradation of redox properties, and (iv) gas leakage between the two reactors. These challenges can be effectively overcome if gases rather than solids are circulated between the two reactors using a manifold switching system. However, before the MSR concept can be implemented, one needs to examine its technical viability by examining its impact on the redox reaction of metal oxide oxygen carriers.

3. EXPERIMENTAL SETUPS

One of the key objectives of this project is to establish technical competency in designing large-scale CLAS and ICLAS systems based on a range of key operating parameters and system requirements. To achieve this, one needs to develop relevant design specifications based on the so-called "scale-up" rules which are typically obtained using a range of experiments and theoretical results. We have been examining the impact of manifold switching reactions (MSR) on metal oxide reactivity using two experimental setups with two different sets of characteristic dimensions; enabling us to examine the scale-up effects. These setups are: (a) a bench-scale fixed-bed unit, and (b) a 10 kW_{th} dual fluidised-bed pilot-plant. These setups are briefly discussed in the following sections.

3.1 Bench-Scale Fixed-Bed Unit

The bench-scale fixed-bed setup is used in reaction reactivity studies (i.e. reaction kinetics). More specifically, the fixed-bed setup is used to experimentally determine the pre-exponential factors and reaction orders by fitting the experimental values of reaction times associated with 50% and 100% conversion. As shown in Figures 4 and 5, the fixed-bed setup consists of: (a) a quartz tube reactor externally heated by a tube furnace, (b) a steam generator; (c) a data acquisition system; (d) a gas analysis train comprising a micro-GC, a drying tower and a vent; and (e) a gas inlet manifold which includes several mass flow controllers, three-way valves, regulators and gas bottles.

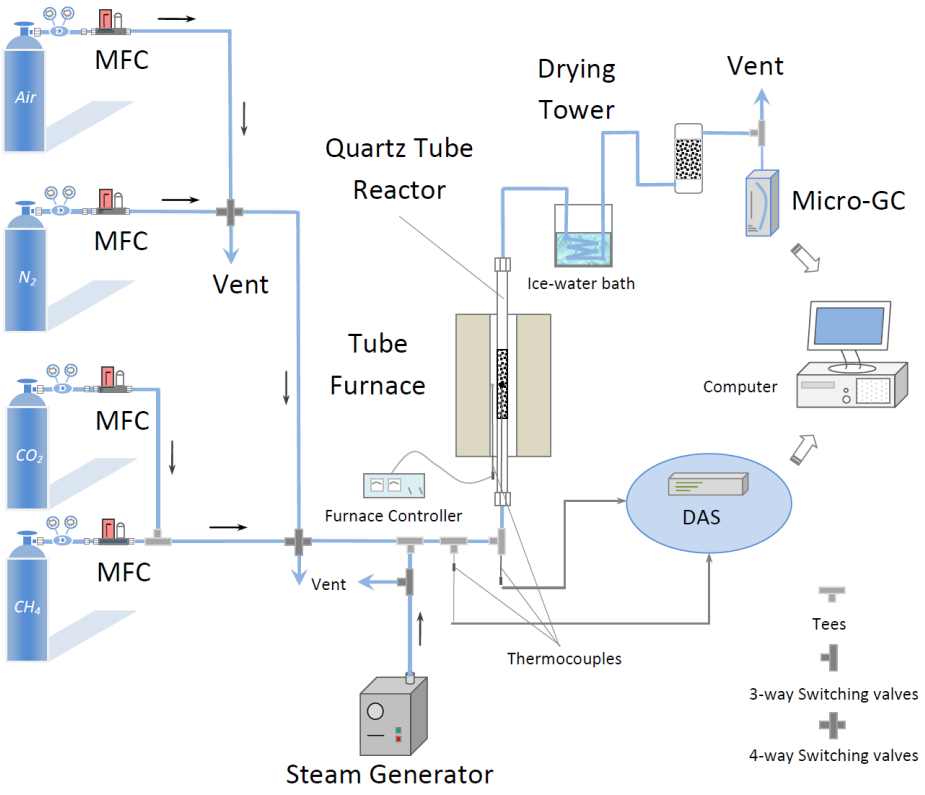

Figure 4: Schematic of the bench-scale fixed-bed setup.

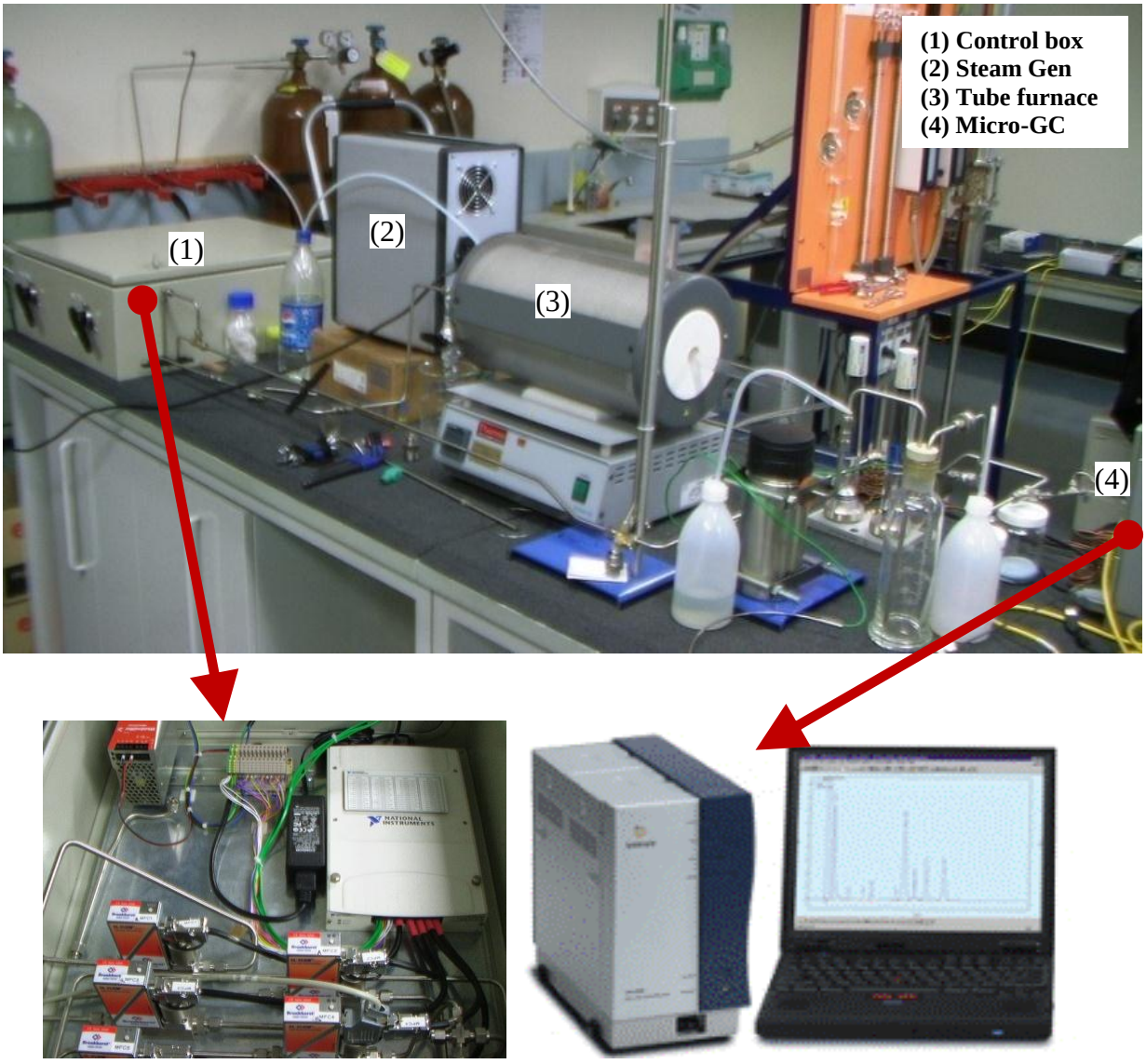

Figure 5: Photos of the bench-scale fixed-bed setup.

3.2 The 10 kW_{th} Pilot-Plant

3.2.1 Dimensional Analysis and Pilot-Plant Design

Dimensional analysis is a powerful theoretical method allowing the performance characteristics of an engineering system to be related with the characteristics of its scaled model run under a different set of operating conditions. Using dimensional analysis we have been able to relate the experimental data collected from the cold-flow and fixed-bed setups and determine the design specifications (e.g. size, geometry, operating temperature, etc) of the 10 kW_{th} pilot-plant. This has been achieved by maintaining identical values of several key dimensionless parameters in bench- and pilot-scale units.

The dimensions of the pilot-scale unit were calculated from those of the bench-scale setup. The key dimensionless parameters used in this analysis were:

$$\frac{u^2}{g.L},\quad \frac{\rho_p}{\rho_f},\quad \frac{\rho_p.u.d_p}{\eta^2},\quad \frac{\rho_f.u.L}{\eta},\quad \frac{G_s}{\rho_p.u},\quad bed\_geometry,\quad \Phi,\quad PSD \qquad (1)$$

where u is superficial gas velocity, g the acceleration of gravity, L characteristic length, ρ_p particle density, ρ_f gas density, d_p particle diameter, η dynamic viscosity of the gas, G_s solid circulation rate, Φ particle sphericity, and *PSD* the particle size distribution.

The original plan was to design and construct a 100 kW_{th} pilot-plant. However, dimensional analysis revealed that the overall footprint of such unit would be about 10×6×8 m; with a capital cost much greater than what was allocated in the budget for the construction of the pilot-plant. For this reason, a new set of dimensional analyses was carried out to assist with the design of a smaller 10 kW_{th} pilot-plant with an approximate footprint of 2.5×1.5×2. The smaller unit size enabled us to design and construct (see next section for details) two versions of the pilot plant, namely: (i) the Perspex version for carrying out hydrodynamic and particle transport studies at pilot-scale, and (ii) the stainless steel or SS version for conducting redox reactions at pilot-scales. Both Perspex and SS versions have identical geometry and dimensions. The design specifications for these pilot-scale units are given in Table 1.

Table 1: Basic design specifications obtained from dimensional analysis for pilot-scale unit(s)

Design Parameter	**Unit**	**Design Specs** (Perspex unit)	**Design Specs** (SS unit)
Thermal power	kW	--	100
Operating temperatures	^oC	Room Temp	650 - 1100
Operating pressure	bar	1	1 - 4
Particle density	kg/m^3	500-2000	2500 - 5400
Mean particle diameter	μm	300 - 400	100 - 200
Dimensionless gas velocity in the riser	--	4 -10	4 -10
Dimensionless gas velocity(oxidation reactor)	--	1-3	1-3
Dimensionless gas velocity (reduction reactor)	--	5-15	5-15
Dimensionless gas velocity in the loop seal	--	1.2 - 4	1.2 - 4
Reactor diameter	m	0.05	0.05
Reactor height	m	0.85	0.85
Total system height	m	2.0	2.0

3.2.2 Design and Specification of the Pilot-Plant

The design and construction of the dual 10 kW_{th} pilot-plant has been a vital component of the work completed to date. The plant, as shown schematically in Figure 6, consists of: (a) a dual fluidised bed

reactor (essentially a pair of interconnected fluidised bed reactors) externally heated by two tube furnaces, (b) steam generator, (c) inlet gas manifold comprising gas bottles, mass flow controllers, three-way valves and piping & fittings, (d) gas analysis train comprising a condenser, drying tower, a micro-GC and a vent, (e) cyclones and feeders, and (f) control box.

(a) (b)

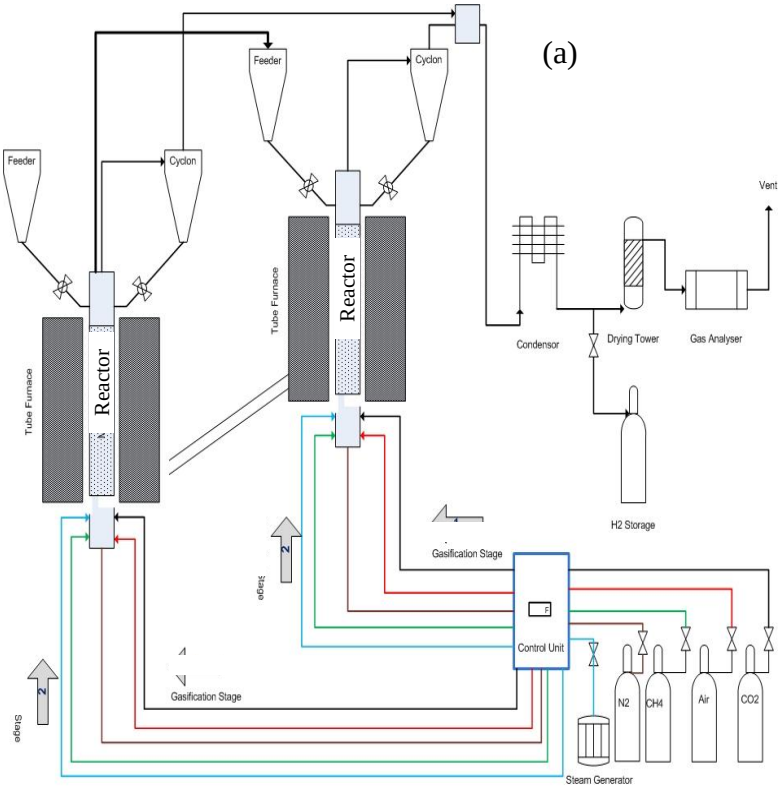
Feeder
Cyclon
Feeder
Cyclon
Vent
Tube Furnace
Reactor
Reactor
Tube Furnace
Condensor
Drying Tower
Gas Analyser
H2 Storage
Gasification Stage
Control Unit
Gasification Stage
N2
CH4
Air
CO2
Steam Generator

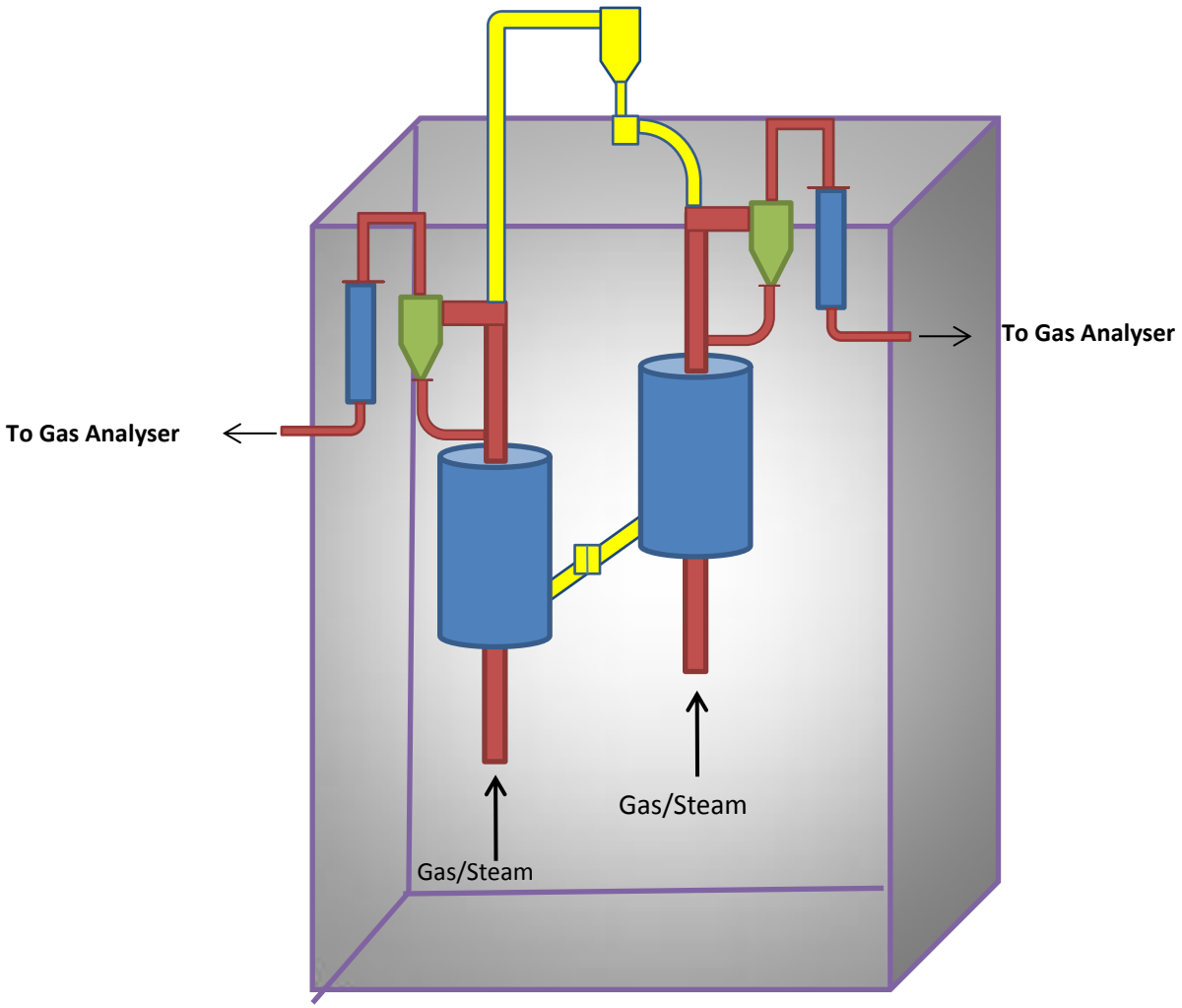

Figure 6: Schematic of the pilot-scale setup; (a) 2D view, and (b) 3D view.

Two different versions of the pilot-plant were constructed as part of this study, namely Perspex and SS. The two versions of the pilot-plant have identical components, geometry, configuration and size and only differ in the material of construction for the dual fluidised bed components. In the Perspex version the reactor vessels are fabricated from acrylic materials whereas in the SS version the reactor vessels are constructed from stainless steel. The relevant tasks for construction of the Perspex version of the pilot-plant were completed late Oct, 2011. The Perspex vessels within this version were recently replaced by new reactors fabricated from stainless steel (SS) after the completion of the pilot-scale hydrodynamic experiments. The setup which is shown in Figure 7:

- Can operate in fixed or fluidized bed modes
- Can operate in single or dual reactor configuration
- Can operate in the manifold switching mode where gases rather than particles are circulated
- Can operate over a range of temperatures between 25-1200˚C and pressures up to 20 bar

Figure 7: Pilot plant; (a) full assembly, (b) full assembly front view, (c) enlarged view of a Perspex vessel and tube furnace, (d) control box, (e) internal view of the control box.

The operation of the pilot-plant in dual fluidised bed or manifold switching modes is achieved by manipulating a series of three-way and solenoid valves attached to the system. Figure 8 illustrates the basic configuration of the pilot-plant and how various functionalities can be achieved.

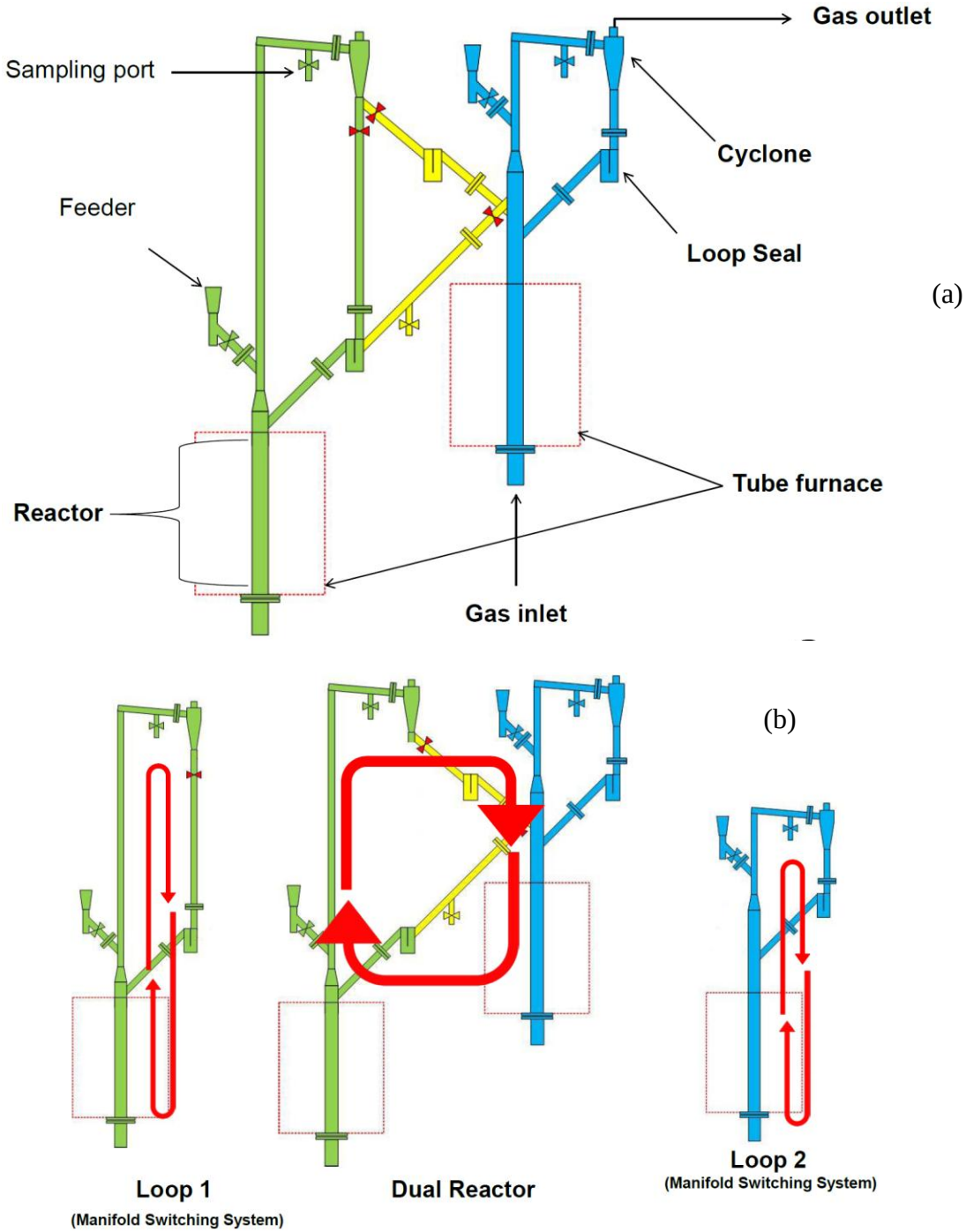

Figure 8: Pilot plant; (a) basic configuration, (b) particle and gas flow arrangement corresponding to various operational modes.

The operational parameters and configuration of the pilot-plant can be easily set to match any desired mode of operation by selecting the relevant system parameters through the LabView user friendly interface which is entirely graphical. Some of the pop-up menus of the LabView interface designed by our team for the 10 kW_{th} pilot-plant are shown in Figure 9.

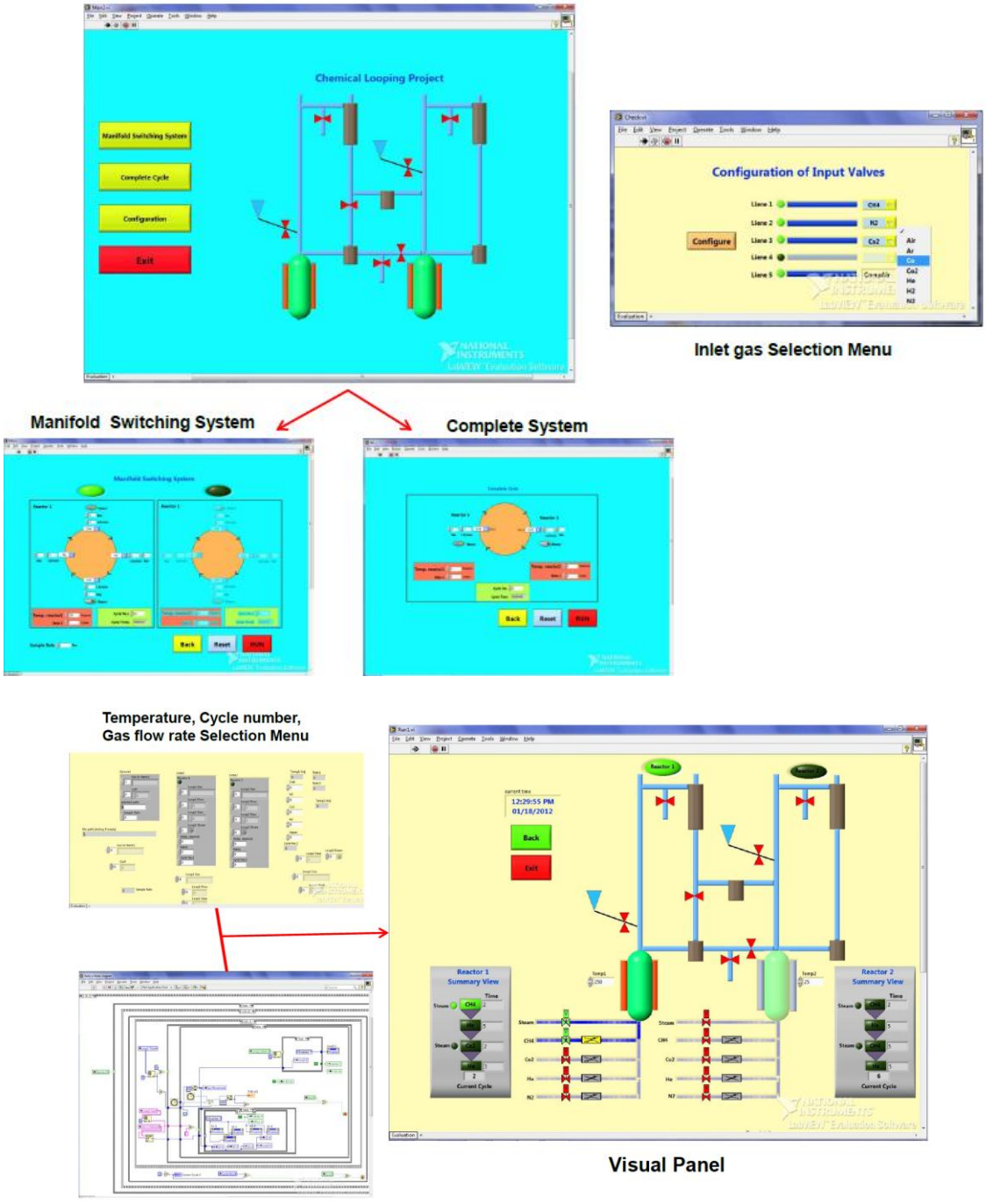

Figure 9: Selection of operational modes/parameters and pilot plant control through the graphical LabView interface.

4. RESULTS AND DISCUSSION

4.1 Fixed-Bed Experiments

4.1.1 Methods and Procedures

The weight of oxygen carrier samples used for fixed bed tests was about 2.5 g. The samples were first loaded into the middle of the quartz tube reactor with outside diameter 7 mm and 1mm wall thickness (see Figure 10). A small amount of quartz wool was then packed to the front and back ends of the sample to fix the sample in place. The tube furnace was employed to heat the samples up to desired temperature at a flow of 40 ml/min air in order to ensure all the particles completely oxidized under isothermal conditions. Once the desired temperature reached, gases were manually switched through four way valves between nitrogen during desorption and a mixture gas with 5% oxygen concentration from air and nitrogen for the adsorption process. The use of nitrogen rather than steam or CO_2 which are the typical reducing agents in CLAS and ICLAS processes was a safety precaution in bench-scale settings. The gas flow rate for both adsorption and desorption was set to 40 ml/min. The low concentration of oxygen was chosen during adsorption for avoiding the high temperature variation caused by the exothermic oxidizing reaction under air. Moreover, this value was also kept greater than the equilibrium partial pressure. This is essential to oxidize the reduced copper oxides at 950^{o}C based on thermodynamic calculations (4.53% by HSC Chemistry Software 6.0). Experiments were carried out in temperature range between 800^{o}C and 950^{o}C. Micro gas chromatograph from Varian equipped with a column of 5A molecule sieve was used to analyse the gases from the outlet of the reactor. The summary of major findings is presented below.

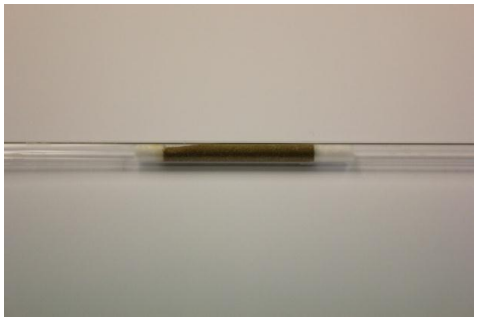

Figure 10: Photograph of the quartz tube reactor loaded with a metal oxide sample.

4.1.2 Fixed-Bed Results for 48%CuO/ SiO_2

Before carrying out the actual tests, a series of experiments was conducted using silica (inert support) to find out if this inert material influences the oxygen adsorption/desorption process in any shape or form. As shown in Figure 11, for this case a small quantity of oxygen with concentration around 0.21% remains in the reactor when switching the reacting gas from 5% O_2 to nitrogen at all temperatures of interest from 700^{o}C to 950^{o}C. Given the long residence times needed for complete removal of this residual oxygen and considering that the influence of such minute quantities of oxygen on the desorption process are negligible, the desorption process in the actual tests was considered complete when an oxygen concentration of 0.21% was reached.

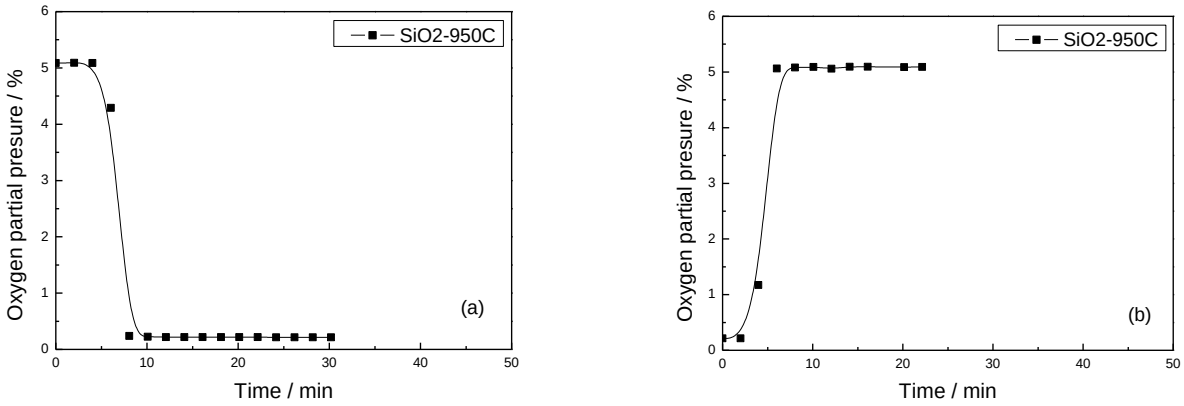

Figure 11: The variation of oxygen concentration tested with silica after (a) switching gas from mixing gas with 5% O_2 to nitrogen; and (b) from nitrogen to mixture gas.

The impact of oxygen partial pressure on the desorption process at temperatures of 800°C, 850°C, 900°C and 950°C are shown in Figures 12 to 15, respectively. In these figures the process of desorption has been expressed as a plot of oxygen partial pressure versus time. Figures 12 to 15 have several common features and clearly illustrate various stages of the desorption process which are described below.

Initial-Lag Phase: As can be seen from Figures 12-15, there is an initial period during which the partial pressure of oxygen measured at the reactor outlet remains at about 5% (the concentration of oxygen in the reactor before switch over to N_2). During this period the incoming nitrogen flow is sweeping through the reactor forcing oxygen out. The metal oxide particles cannot release their oxygen during the Initial-Lag phase because the oxygen concentration is too high (see below for a more detailed explanation). The duration of the Initial-Lag phase depends on the reactor temperature and varies between 10 min at 800°C to about 25 min at 950°C (note that at 950°C the gas volume is much bigger than that at 800°C).

Rapid-Drop Phase: The initial lag is followed by another phase in which the concentration of oxygen rapidly drops to levels close to the equilibrium partial pressure of oxygen. According to our thermodynamic analysis the equilibrium partial pressures of oxygen at 800°C, 850°C, 900°C and 950°C are 0.30%, 0.46%, 1.51% and 4.53%, respectively. As shown in Figures 12-15 for the reactor temperatures of 800°C, 850°C, 900°C and 950°C the actual oxygen partial pressures plunge to values of 0.40% 0.69%, 1.72% and 4.70%, respectively at the end of Rapid-Drop phase. These two sets of values are clearly very close to each other which is essentially what is required for oxygen desorption (i.e. the next phase; see below). The duration of the Rapid-Drop phase appears to be independent of the reactor temperature and is about 5 min when our experimental setup is used (see Figures 12-15).

Oxygen-Uncoupling Phase: Once at a given reactor temperature the actual oxygen partial pressure is lowered to levels close to its corresponding equilibrium partial pressure, the dynamics of the redox reaction shifts in the reverse direction forcing metal oxide particles to relinquish their oxygen. During this phase metal oxide particles effectively become emitters of oxygen helping to maintain a relatively

constant oxygen partial pressure in the reactor outlet (see Figures 12-15). The oxygen-uncoupling phase can last as long as sufficient quantities of metal oxide particles exist in the reactor.

Extinction Phase: Once all metal oxide particles release their oxygen molecules and reduced to a lower oxidation state, the oxygen-coupling phase ends and the oxygen concentration in the reactor outlet rapidly drops to values close to zero (i.e. nitrogen only). This period, which is named here as the "Extinction" phase, is shown in Figure 15 for the reactor temperature of 950°C. As can be seen for at this temperature the Extinction phase commences after about 65 min of operation. The Extinction phase is not shown in Figures 12-14 for reactor temperatures of 800°C, 850°C, and 900°C given that these figures only show up to 45 min of operation (at these temperatures the extinction commences around 55 min).

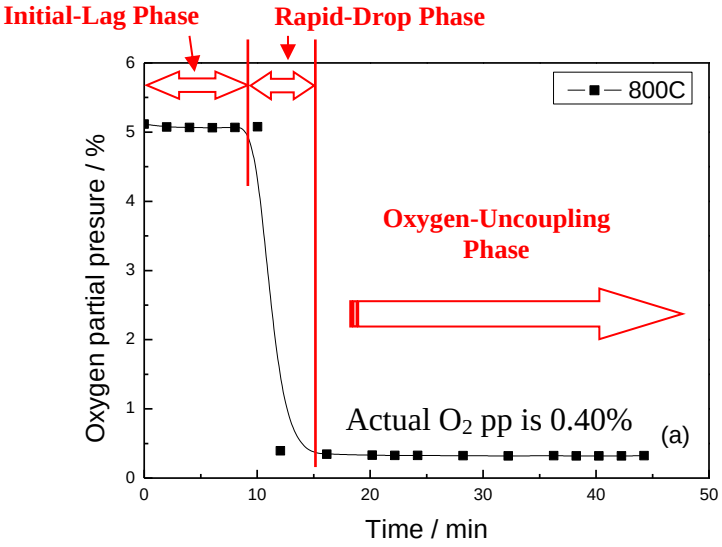

Figure 12: The variation of oxygen partial pressure during desorption under N_2 at 800°C.

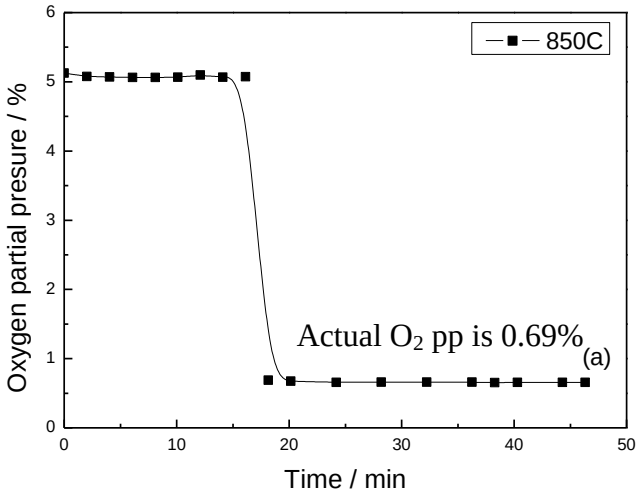

Figure 13: The variation of oxygen partial pressure during desorption under N_2 at 850°C.

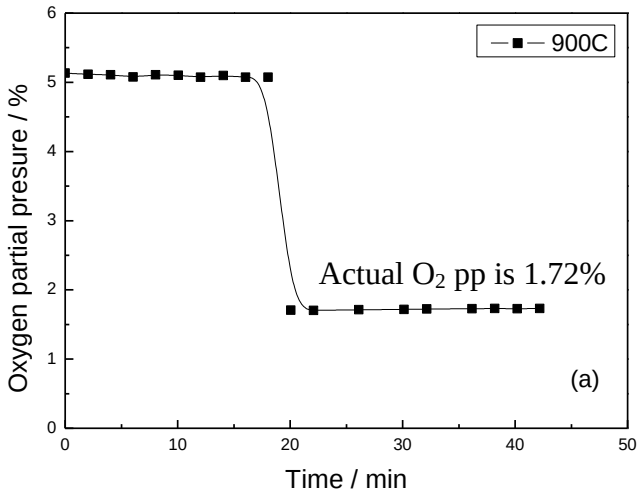

Figure 14: The variation of oxygen partial pressure during desorption under N_2 at 900°C.

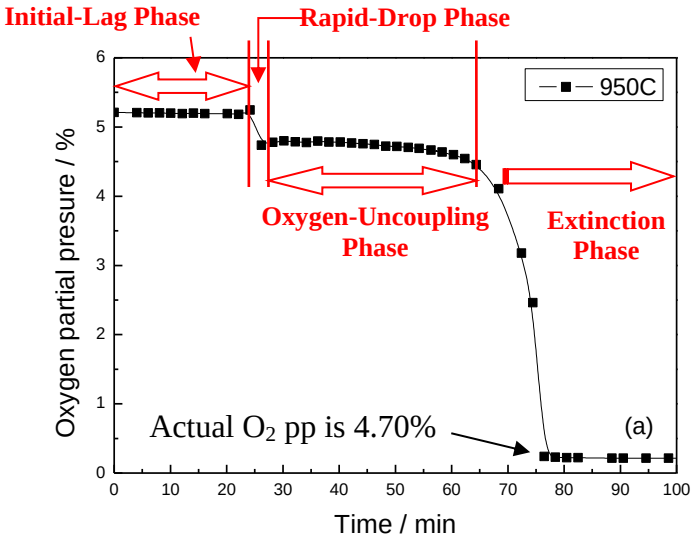

Figure 15: The variation of oxygen partial pressure during desorption under N_2 at 950°C.

4.2 Pilot - Plant Experiments

4.2.1 Working Principle

The working principle of the manifold switching process is very simple. Unlike conventional chemical looping processes, in manifold switching the solid reactants are stationary. The process is carried out using two reactors operating in opposite modes, that is, one reactor undergoes oxidation while the other is under reduction. Once the solid reactants have been fully converted to products, the inlet gas streams

are switched between oxidation (i.e. air) and reduction agents (e.g. steam, CO_2, flue gas, etc) to change the operating mode of the reactors. To avoid undesirable mixing of the oxidation and reduction agents a pulse of a swipe gas (e.g. He) is introduced to each reactor prior to every switching cycle.

Figure 16 schematically illustrates the evolution of the concentration and temperature fields within the MSR unit. As shown, initially the metal oxide particles are un-reacted since the sweep gas which is initially introduced into the reactor is non-reactive. As a result, the whole system is at a uniform initial temperature. Once the reactive gases are introduced into the MSR unit, heterogeneous reactions between particles and the gas begin and consequently a reaction front with a rate of W_1 propagates through the bed. Due to chemical reactions the bed temperature changes (see Figure 16b). This change leads to a difference between the bed and incoming gas temperatures, in turn, giving rise to a heat front which travels through the bed at a rate of W_2.

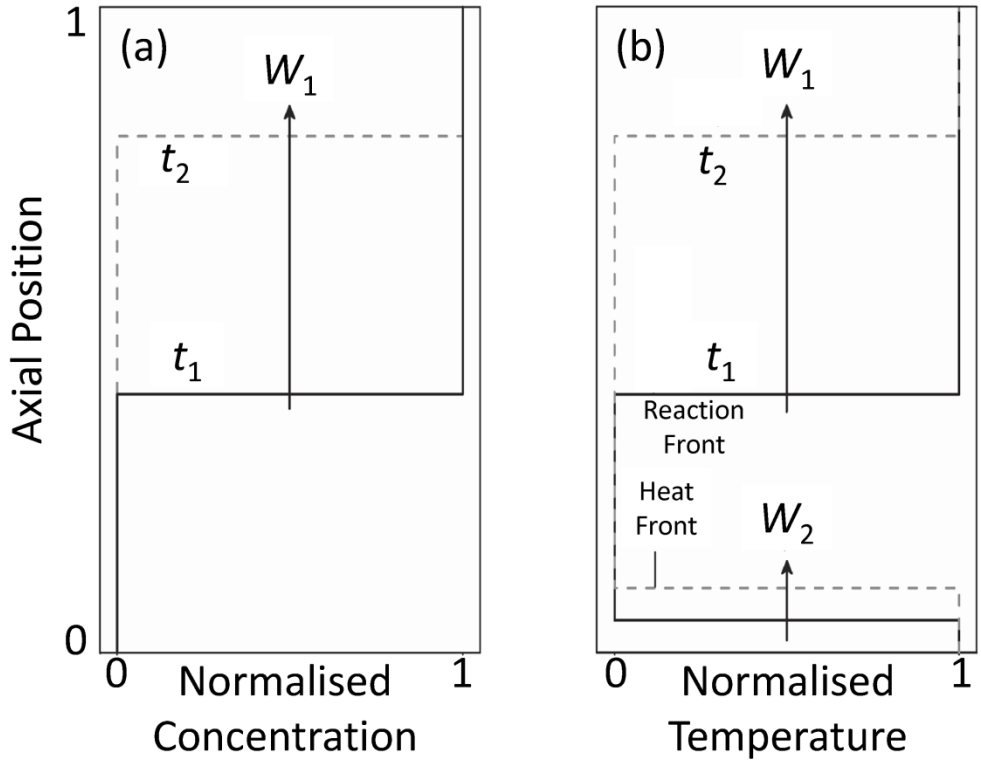

Figure 16: Schematic representation of the evolution of the normalised fields for (a) concentration of product gases and (b) bed temperature within a typical MSR unit.

4.2.2 Experimental Methods & Techniques

Oxides of Cu(II) on alumina support were employed in MSR experiments. The preparation of the metal oxide samples begun by the direct mixing of commercial CuO powders (Sigma-Aldrich) with alumina powder (Sigma-Aldrich) at a 3:2 carrier/support weight ratio. Distilled water was then added to the carrier/support mix to form a paste. The paste was dried in an oven at 105^{o}C for 36 hours to free up the

capillary water. The dry paste was then calcined for 5 hours under nitrogen in a high temperature furnace at a set temperature of 750^{o}C. The calcined sample was pulverised in a ball mill and sieved to a particle size range of 90-106 μm (mesh 170 < particle size < mesh 140[§]). The quality of the final products were evaluated using X-Ray fluorescence (XRF) and X-Ray Diffraction (XRD) methods to determine the distribution of metal active sites on the surface and within the carrier particles, respectively. The internal structure of samples were characterised by mercury porosimetry and BET (Brunauer-Emmer-Teller) surface area measurements. In particular, the thickness of platelike grains of the CuO layer was determined from the weight fraction of CuO in the sample and the active surface area data. Table 2 summarises the physical characteristics of the oxides prepared in this study.

Table 2: Properties of CuO on alumina support

Property	Unit	CuO
Actual active metal oxide content	%wt	62
Molecular weight of the active metal oxide	kg kmol^{-1}	79.55
Solid density	kg m^{-3}	4200
Molar density of the active metal oxide	mol m^{-3}	32734
Particle size	μm	90 to 106
Porosity	--	0.6
BET specific surface area	m^2 g^{-1}	44
Grain size	m	--
Thickness of the metal oxide layer (CuO samples only)	m	1.22×10^{-8}

The experimental setup shown in Figures 6 and 7 was employed to carry out a comprehensive set of MSR experiments. A total of 20 thermocouples were fitted along the length of both reactors so that the axial temperature distribution can be measured with a high degree of spatial resolution. Similarly, 10 iso-kinetic sampling ports were fitted to each reactor for collection of gaseous reactant and products along the reactor length at 1 min intervals. Collected gas samples were analysed using a micro-GC unit. The reactors were externally heated by two tube furnaces. Insulation materials were inserted between the furnace and reactor walls to minimise radial heat losses.

A typical experiment consisted of several redox (reduction / oxidation) cycles to allow the sample to stabilise. Typically the data set corresponding to the fifth redox cycle was used for determination of reaction data since the redox properties of the sample considerably deteriorated over the first few cycles until they reached a repeatable level at or on about the fifth cycle. The experimental procedure involved the following steps: (i) a charge of between 250 to 500 g of metal oxide was loaded into each reactor, (ii) the heating system was turned on and the reaction temperature was set to a pre-determined level, (iii) the reactor was then purged with nitrogen and the sample was heated under nitrogen at a rate of 100^{o}C/min, (iv) once the desired temperature was reached the nitrogen flow was turned off and instead the reacting gases were introduced, (v) the samples were then allowed to react with the gas

§ *ASTM-E11 standard*

mixture until the changes in the concentration of products at the outlet of each reactor diminished, (vi) at this point the flows of reacting gases were stopped and a purge of He was introduced for about 10 s to avoid the mixing of air and reducing gas, (vii) steps iv to vi were repeated at least three times and the measurements of temperature distribution and product concentration corresponding to the final redox cycle (typically fifth cycle) were collected for further analysis.

4.2.3 Results

Figures 17 and 18 show the temporal and spatial distributions of the oxygen concentration and gas temperature in a MSR unit during a typical oxidation half cycle. From these figures the propagation of the reaction front can be easily observed. It is also clear from these figures that the oxidation reaction precedes at a sufficiently high rate. The reference to "sufficiently high" rates is made in the context of comparing the fixed-bed results presented in Figures 11-15 and manifold switching results presented in Figure 17. For instance, as can be seen from Figure 11 it takes about 10 min (@95^{o}C) in the fixed-bed setup to reach a 100% oxidation conversion whereas in the manifold switching reactor the same process takes about 4 min (see Figure 17).

Figure 18 in particular indicates that the high oxidation rate results in a relatively steep temperature front and that the temperature rise appears to be uniform over the reactor length. The shape of the temperature profiles over the regions where temperature is decreasing (e.g. axial positions between 0.7 and 1 m for the 4 min plot) is an indication of radial heat losses although our analyses confirm that the effect of such losses in the centre of the reactor in a given redox cycle is about ±8 which is quite negligible.

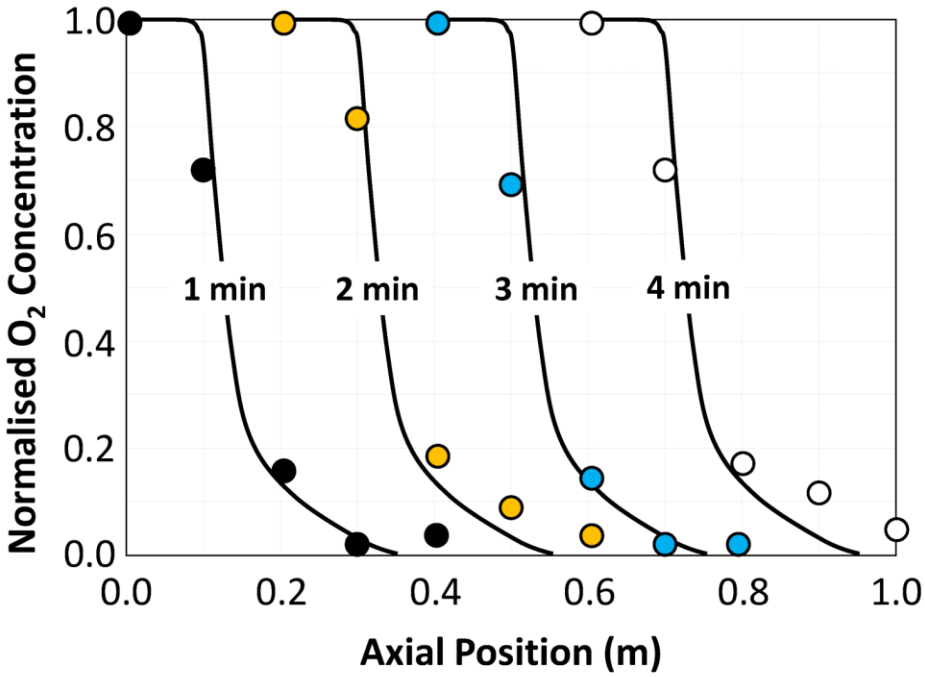

Figure 17: Temporal and spatial evolution of the normalised oxygen concentration within a typical MSR unit.

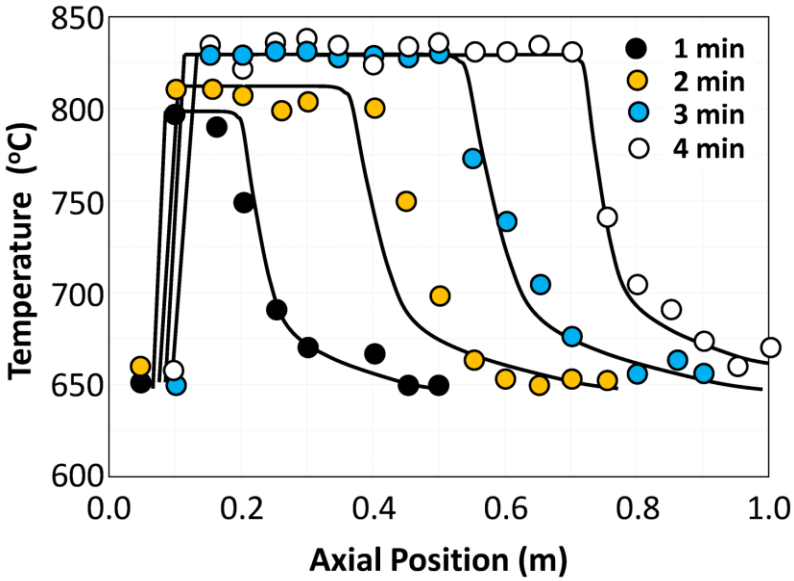

Figure 18: Temporal and spatial evolution of the temperature within a typical MSR unit.

Figure 19 illustrates the temporal variation of the gas temperature at the reactor outlet for a complete oxidation half cycle. As can be seen, the temperature profile is not completely uniform when the oxidation half cycle begins primarily as a result of residual heat (i.e. preheating) from the previous reduction half cycle. A careful analysis of all experimental data has indicated to us that while such small temperature effects may be eventually levelled out, they usually lead to larger deviations from the desired temperature profiles and hence lower the overall effectiveness of the manifold switching process. These temperature effects can be cancelled out either by increasing the reactor length which effectively increases the residence time of the heat front in the bed, or by mild fluidisation of the particle bed for a relatively short period of time just after the completion of the proceeding half cycle.

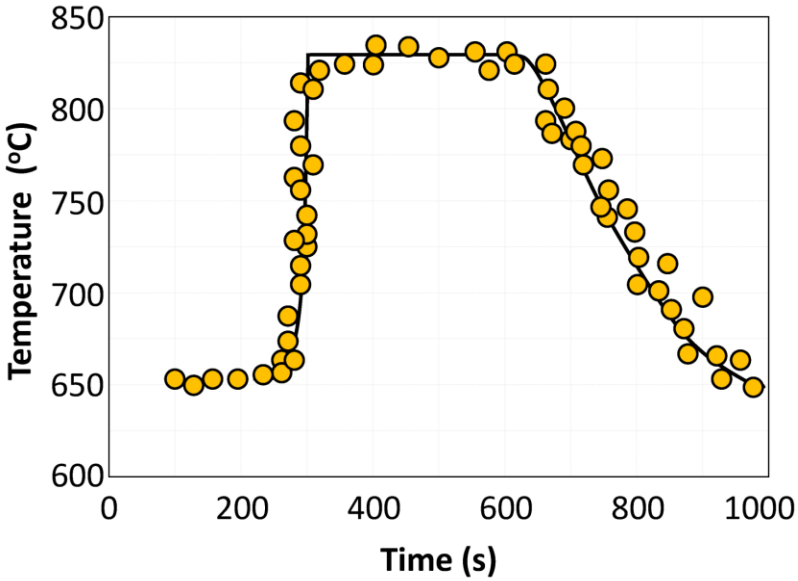

Figure 19: Variation of the reactor outlet temperature as a function of time within a typical MSR unit.

Figure 20 shows plots of maximum temperature rise (that is the difference between the initial and maximum temperatures at a given axial location in a typical reaction half cycle against reactor length for three different cases. The base case refers to results corresponding to a residence time of 15 min under standard operating conditions. However, in the "increased flow rate" case the volumetric flow rate of the incoming gas has been increased by a factor 5 (gas velocity was kept just below the minimum fluidisation velocity). All other parameters and variables for this case were identical to the base case. Similarly, in the "decreased reactivity" case the metal oxide particles were doped with a layer of inert material to lower their reactivity by a factor 2. Again, all other parameters and variables for this case were kept the same as the base case.

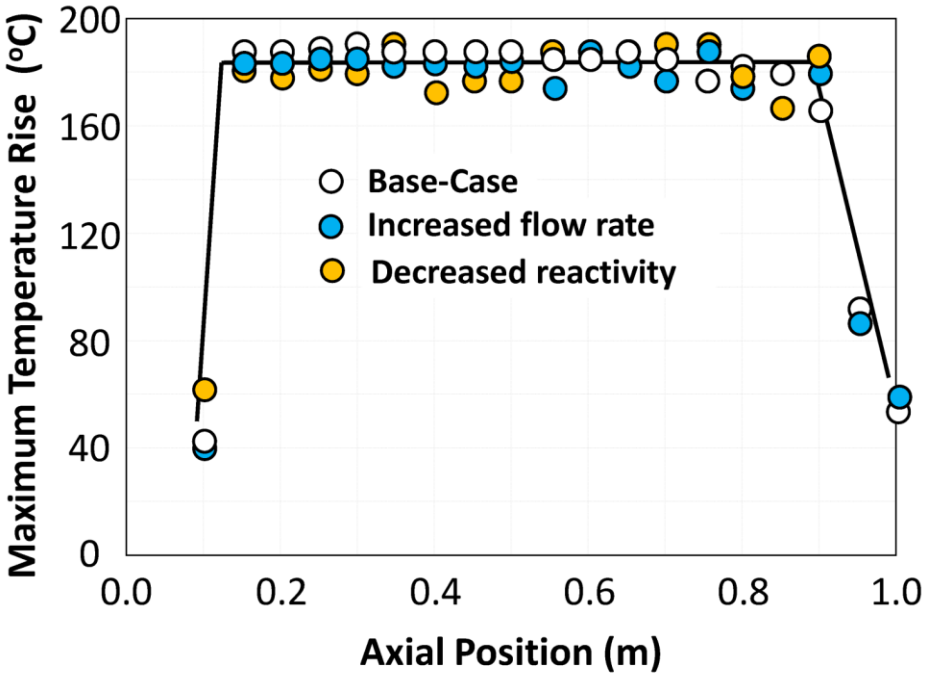

Figure 20: Plots of maximum temperature rise as a function of the axial position for a typical MSR unit.

The plots shown in Figure 20 indicate that maximum temperature rise is neither sensitive of to the gas flow rate nor reaction kinetics given that plots for all three cases are almost identical. This is perhaps the most important finding of MSR studies as it implies that the reactor temperature profile is not a function of reaction kinetics or gas flow rate, but only of the properties of gas and solid material. We have verified this finding through a simple analytical analysis which resulted in the following expression:

$$\Delta T = \frac{-\Delta H_{\mathrm{R}}}{\dfrac{C_{p,\mathrm{s}} M_{\mathrm{act}}}{w_{\mathrm{act}} \xi} - \dfrac{C_{p,\mathrm{g}} M_{\mathrm{O}_2}}{w_{\mathrm{g,O}_2}^{\mathrm{in}}}} \qquad (2)$$

where

- ξ represents the ratio of the number of moles of gas and solid needed for the oxidation reaction
- w_{act} denotes weight fraction of the reactive material in the oxygen carrier
- $C_{p,s}$ and $C_{p,g}$ are the specific heats of solids and gas respectively
- $w_{g,O2}^{in}$ is weight fraction of the reactive component in the gas
- M_{act} and M_{O2} are molecular weights of reactive component of the solid and oxidation agent (air) respectively
- ΔH_R is the reaction enthalpy

From a process operation and safety point of view such independence from reaction kinetics and flow rate is very advantageous. Therefore, as long as the oxidation reaction is fast enough, any potential decrease of the activity of the oxygen carrier will not directly affect the reactor temperature and temperature rise. This suggests a system with high degree of stability and robustness to deal with an industrial level of variability.

5. CONCLUSIONS

Unlike conventional chemical looping systems, in MSR based systems carrier particles are not circulated between the two reactor assemblies and the cycle is completed by switching over the reacting gases from one reactor assembly to the other. Each reactor, therefore, functions periodically as a fuel reactor and an air reactor. As a result the oxygen carrier particles are not subjected to cyclic moves from one reactor to another and, hence, their physical integrity can be maintained over a much larger of repeated redox cycles. This opens up a pathway for a much wider use of low mechanical strength yet highly effective oxygen carriers for chemical looping air separation. The experimental results presented in this report have certainly confirm the strengths of the manifold switching concept and demonstrated that the technique has no detrimental impact on the cyclic redox reactions between oxygen carrier particles and air. However, the use of packed beds in MSR units may lower the degree of mixing in the reactors and ultimately lead to formation of undesirable hot spots in the reactors. This however can be resolved if packed beds are periodically subjected to mild fluidisation.

6. ACKNOWLEDGEMENTS

The authors wish to thank other members of the Chemical Looping Research group at the University of Newcastle (Dr Luo, Dr Peng, Mr Alghamdi, Ms Paymooni, Mr Wilson and Mr Zhang) for their hard work and dedication as well as contributions to the present report. The authors would also like to acknowledge the financial support provided to this project by the NSW government through the Coal Innovation NSW fund as well as Xstrata Research Pty Ltd.